Generating realistic trajectories for robotic hippotherapy from 3D captured horseback motion

Jakob Ziegler[1], Hubert Gattringer[1], Alexander Reiter[1], Philip Hörmandinger[1], Andreas Müller[1] and

Markus Mitterhumer[2]

[1] *Institute of Robotics, Johannes Kepler University Linz,* {*jakob.ziegler,hubert.gattringer,alexander.reiter,a.mueller*}*@jku.at*
[2] *intelligent motion gmbh*

ABSTRACT — *Riding a horse is a complex movement that is cognitively and physically demanding. It is established as a rehabilitation method for improving postural stability and locomotion performance, also known as hippotherapy. To facilitate the application in clinical environments, robotic hippotherapy systems have recently been developed. A therapy outcome equivalent to classical hippotherapy requires the robotic horse trajectories to be as close to reality as possible. In order to generate realistic trajectories executable by robotic systems, this work focuses on the synthesis of horseback motions based on 3D motion capture data. Representing the saddle of a therapy system, the horseback is treated as a rigid body. A marker selection approach is introduced to extract the data most significantly describing the rigid body motion of the horseback. The position and orientation components of the movement are determined by a least squares point matching algorithm and are approximated by Fourier series in order to generate smooth, cyclic and realistic trajectories effectively executable by robotic systems.*

1   Introduction

Therapeutic horseback riding, also called equine assisted therapy (EAT) or hippotherapy, is a medical treatment used for persons with movement disorders that is based on the interaction of the rhythmic, dynamic movement of the horse with the rider. Riding a horse is a complex movement that is cognitively and physically demanding, with significant similarities to human walking [1, 2]. The provided sensory stimuli have positive rehabilitational effects on the human body. Hippotherapy has, amongst others, successfully been applied to improve gross motor function [3], postural control [4], balance [5], muscle symmetry [6], trunk/head stability and functional reach [7], as well as for post-stroke gait training [8].

As a part of the demographic change, life expectancy is currently increasing. Therefore, the worldwide population is growing older combined with a greater risk of age-related diseases. Due to the rising demand for movement rehabilitation, there recently has been an increasing interest in robotic rehabilitation devices to support traditional therapy approaches. The possibility to facilitate hippotherapy in clinical environments or avoiding the necessity of a real horse additionally motivates the development of robotic hippotherapy systems such as e.g. the system *hirob* developed by *intelligent motion* [9]. Furthermore, robotic hippotherapy has the potential to increase the accessibility of this treatment for the patients.

Recent studies reveal that robotic hippotherapy systems have similar rehabilitational effects compared to classical EAT, where real horses are involved [10, 11, 12]. Classical EAT has limited control of the cadence of the movement and is dependent on the temperament of the horse, containing the risk of unpredictable motions. An advantage of robotic hippotherapy systems is the precision of the therapeutic movements with adjustable speed and high repeatability. Nevertheless, in order to improve the sensation of real horseback riding and to deliver a therapy outcome equivalent to classical hippotherapy the robotic horse trajectories have to be as close to the movements of real horses as possible. Existing publications analyzed horse motions on the basis of motion capture data [13], acceleration data [1, 14] or photographs [15].

This work presents the synthesis of the horseback motion during typical horse gaits based on 3D motion capture data by employing a least squares point matching algorithm. As the horseback is treated as a rigid body representing the saddle of a robotic therapy system, a marker selection approach is introduced to extract the data most significantly describing the riding motion. The extracted motion data, i.e. the position and orientation of the horseback with respect to a reference coordinate system, is then approximated in order to generate smooth, cyclic and realistic trajectories effectively executable by robotic systems.

2   Motion capture data

The measurement of the horse movements was done with a marker-based motion capture system and respecting sets of reflective markers attached to two different horses, *Lambada* and *Doolittle*. The provided raw 3D data of the marker coordinates were acquired for three typical horse gaits, depicted in Fig. 1. The *walk* and *trot* motion were recorded for both horses, whereas the *gallop* motion was only recorded for *Doolittle*, giving a total of five motion data sets. Additionally, marker data of the horses in steady standing position were used as reference defining the shape of the respective horseback. In a pre-processing step the raw data of the standing horses are aligned with a reference coordinate frame. First, the markers nearest to the spine of the horse are aligned with the *x* axis, as they approximately represent the center line of the horse body. Then, the marker coordinates are centered around the origin with respect to the *x* and *z*-direction. This procedure defines the reference pose for each horse, as it is shown in Fig. 2.
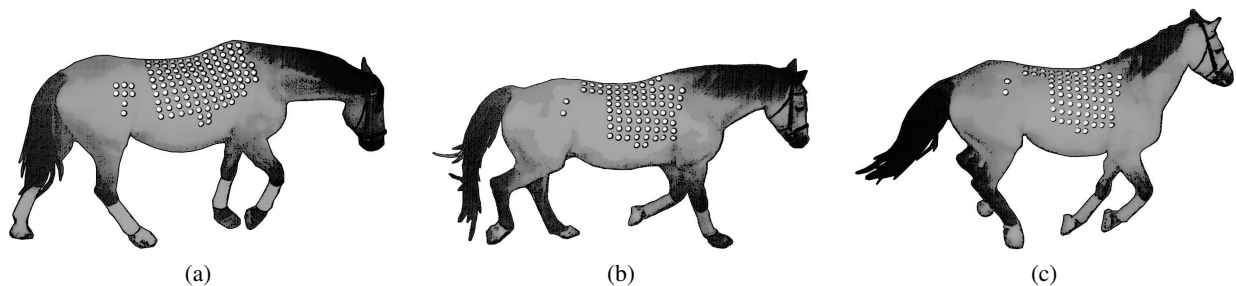

Fig. 1: The three investigated horse gaits: (a) walk, (b) trot and (c) gallop. The marker arrangements on the two horses *Lambada* (a) and *Doolittle* (b,c) are shown as white dots.

Concerning the recorded data of the individual movements, only motion capture snapshots were considered where 90 % of the markers are visible. Since, although each individual marker is uniquely identified during a motion capture run (i.e. within the corresponding data set) but markers have different IDs for different measurements, the marker correspondences between reference pose and motion data set must be determined. To this end, the error of the reference marker positions and the marker positions of the frames of the respective motion data set, where all markers have to be visible and the point sets are centered around $[0,0,0]^\top$, is calculated. A nearest neighbor search between the reference data and the marker positions of the motion data frames yields the marker correspondences of reference pose and motion data set.

The result for each horse and each movement is the data set $\{\hat{\mathbf{r}}_1, \ldots, \hat{\mathbf{r}}_k\}$ of k marker positions in the steady reference pose of the horse and a sequence of N marker data sets $\{\hat{\mathbf{p}}_{1,l}, \ldots, \hat{\mathbf{p}}_{k,l}\}$, $l = 1, \ldots, N$ (one for each of the N snapshots during the respective gait measurement).

3   Marker selection

Considering the marker placement on the horses it is assumed that, while the horse is moving, some markers have a bigger relative movement with respect to their respective reference position than others, which is contrary to the idea of modeling the horseback as a rigid body. Therefore a marker selection based on the positional variance of the markers during the respective horse movement is performed. The markers on the back and the middle of the
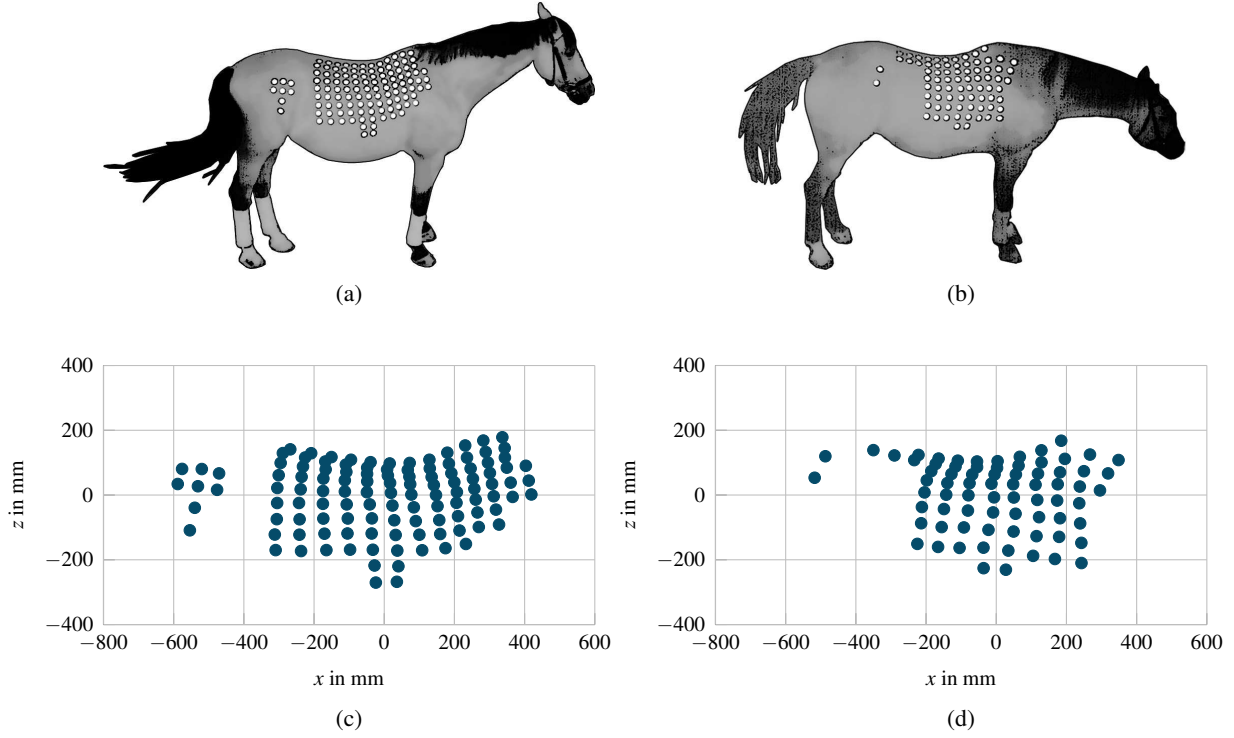
Fig. 2: Arrangement of the 3D markers (white dots) on the horses *Lambada* (a) and *Doolittle* (b), as well as the corresponding 3D data of the markers defining the reference poses (c,d).

flank of the horse are suspected to have smaller variance than the markers near the fore and hind leg, which would be in accordance with the traditional placement of a horse saddle.

The calculation of the positional variance of the markers is based on the marker-to-marker distances $d_{i,j}^{(0)}$ of the reference pose, with

$$d_{i,j}^{(0)} = \|\hat{\mathbf{r}}_i - \hat{\mathbf{r}}_j\|. \tag{1}$$

Accordingly, the marker-to-marker distances $d_{i,j}^{(l)}$ for each of the $l = 1, \ldots, N$ measurements of the movement data set are calculated. The vector of mean differences of the marker-to-marker distances of marker i, $\mathbf{m}_i = [m_i^{(1)}, \ldots, m_i^{(N)}]$, for this movement data set is given by

$$m_i^{(l)} = \frac{1}{k} \sum_{j=1}^{k} |d_{i,j}^{(0)} - d_{i,j}^{(l)}|. \tag{2}$$

Finally, the position variance v_i of all $i = 1, \ldots, k$ markers concerning all N frames of the motion data set can then be calculated as

$$v_i = \frac{1}{N-1} \sum_{l=1}^{N} |m_i^{(l)} - \overline{m}_i|^2 \tag{3}$$

where $\overline{m}_i$ denotes the mean value of $\mathbf{m}_i$. Only markers with a positional variance below a threshold value, e.g. the median variance, are used to extract the horseback trajectory of the respective motion capture data, giving the final sets of marker positions $\{\mathbf{r}_1, \ldots, \mathbf{r}_n\} \subset \{\hat{\mathbf{r}}_1, \ldots, \hat{\mathbf{r}}_k\}$ and $\{\mathbf{p}_{1,l}, \ldots, \mathbf{p}_{n,l}\} \subset \{\hat{\mathbf{p}}_{1,l}, \ldots, \hat{\mathbf{p}}_{k,l}\}$. Based on this approach, Fig. 3 shows the positional variance of the markers for the data set of horse *Lambada* and the walking motion, as well as the resulting selected markers (filled circles). As expected, markers near the front and the hind leg of the horse show a higher relative motion than markers on the horseback. Figure 4 shows the selected markers for the other data sets. Varying from data set to data set some of the markers are missing, as there was no positional information during the specific measurement trial.
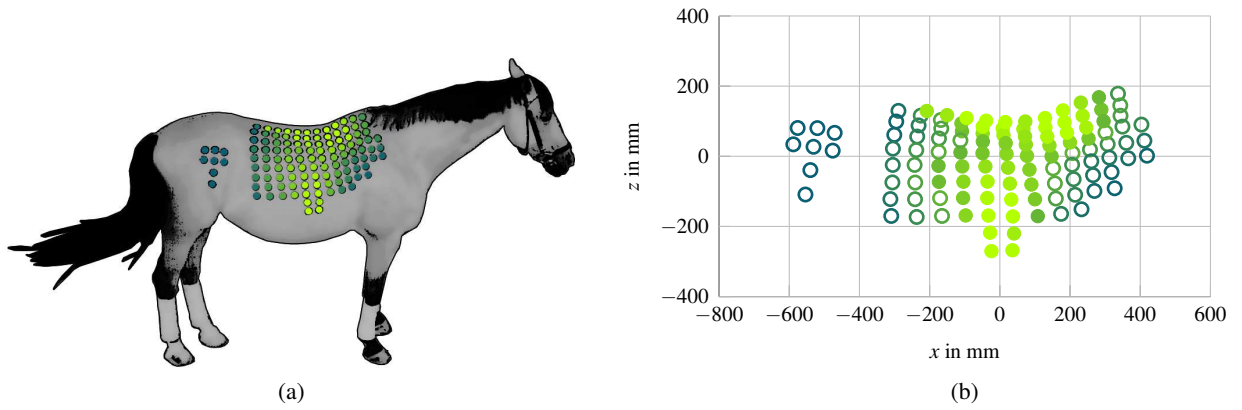
3

Fig. 3: Marker selection for *Lambada* and walking motion. (a) positional variance of the individual markers (dark color indicates high variance, light color indicates low variance) and (b) selected (filled) and ignored (empty) markers based on the variance and a threshold value of this data set.
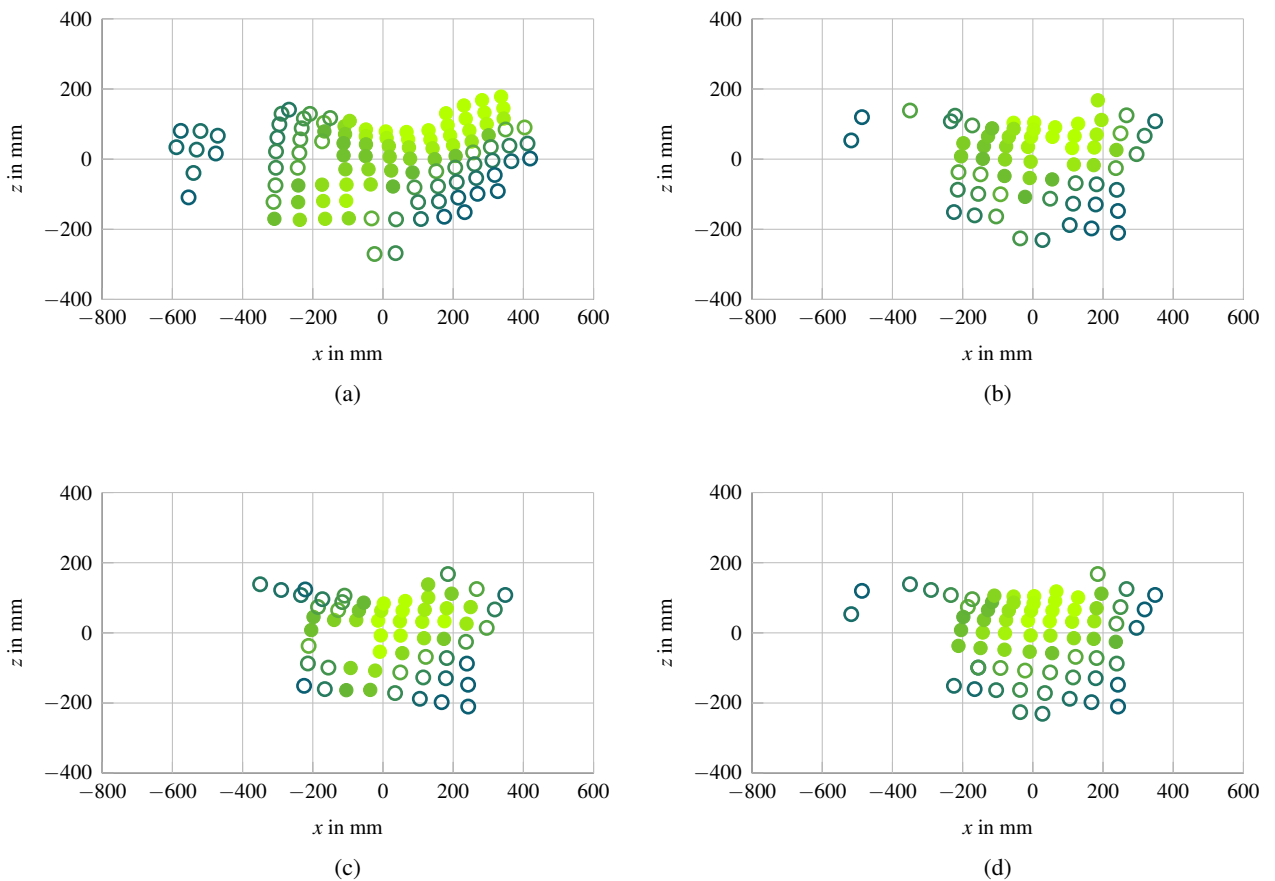

Fig. 4: Marker selection for (a) *Lambada* trotting, (b) *Doolittle* walking, (c) *Doolittle* trotting and (d) *Doolittle* galloping. Based on a threshold value, markers are selected (filled) or ignored (empty) for the respective data set. The color shows the value of the positional variance of the individual markers, where dark color indicates high variance and light color indicates low variance.

4 Trajectory generation

In order to simplify the extraction of the therapeutic trajectory, the horseback is regarded as a rigid body representing the saddle of the robotic hippotherapy system. Therefore, for each marker data set $l = 1, \ldots, N$, the pose of the horseback (as rigid body) relative to the reference pose has to be determined in order to describe the trajectory of the saddle, which can be done e.g. in a least squares sense.

4.1 Least squares rigid motion

The problem stated above amounts to find a rigid body transformation matrix $(\mathbf{R}_l, \mathbf{t}_l) \in SE(3)$, i.e. an 'optimal' rotation $\mathbf{R}_l$ and translation $\mathbf{t}_l$ mapping the marker coordinates $\{\mathbf{p}_{1,l}, \ldots, \mathbf{p}_{n,l}\}$ of frame l to the marker coordinates $\{\mathbf{r}_1, \ldots, \mathbf{r}_n\}$ of the reference pose, so that

$$(\mathbf{R}_l, \mathbf{t}_l) = \underset{(\mathbf{R}_l, \mathbf{t}_l) \in SE(3)}{\arg\min} \sum_{i=1}^{n} w_i \| (\mathbf{R}_l \mathbf{p}_{i,l} + \mathbf{t}_l) - \mathbf{r}_i \|^2, \tag{4}$$

with w_i being weights, e.g. based on the positional variance of the markers. A closed form solution of Eq. (4), also known as weighted orthogonal Procrustes problem [16], is described in [17, 18, 19]. To briefly sum up the approach using singular value decomposition [18, 20], we first assume the rotation to be fixed and denote

$$L(\mathbf{t}_l) = \sum_{i=1}^{n} w_i \| (\mathbf{R}_l \mathbf{p}_{i,l} + \mathbf{t}_l) - \mathbf{r}_i \|^2. \tag{5}$$

The optimal translation can be found by searching for the roots of the derivative of L with respect to $\mathbf{t}_l$:

$$\frac{\partial L}{\partial \mathbf{t}_l} = 2\mathbf{t}_l \sum_{i=1}^{n} w_i + 2\mathbf{R}_l \sum_{i=1}^{n} w_i \mathbf{p}_{i,l} - 2 \sum_{i=1}^{n} w_i \mathbf{r}_i = 0. \tag{6}$$

By denoting

$$\overline{\mathbf{p}}_l = \frac{\sum_{i=1}^{n} w_i \mathbf{p}_{i,l}}{\sum_{i=1}^{n} w_i}, \quad \overline{\mathbf{r}} = \frac{\sum_{i=1}^{n} w_i \mathbf{r}_i}{\sum_{i=1}^{n} w_i}, \tag{7}$$

where $\overline{\mathbf{p}}_l$ is the weighted centroid of the marker positions of frame l and $\overline{\mathbf{r}}$ is the weighted centroid of the reference marker positions, and rearranging Eq. (6), the optimal translation is given as

$$\mathbf{t}_l = \overline{\mathbf{r}} - \mathbf{R}_l \overline{\mathbf{p}}_l. \tag{8}$$

Substituting Eq. (8), that moves the transformed weighted centroid of $\{\mathbf{p}_{1,l}, \ldots, \mathbf{p}_{n,l}\}$ to the weighted centroid of $\{\mathbf{r}_1, \ldots, \mathbf{r}_n\}$, into Eq. (4) and calculating the centered vectors $\mathbf{x}_{i,l} = \mathbf{p}_{i,l} - \overline{\mathbf{p}}_l$ and $\mathbf{y}_i = \mathbf{r}_i - \overline{\mathbf{r}}$ of the point sets results in

$$\mathbf{R}_l = \underset{\mathbf{R}_l \in SO(3)}{\arg\min} \sum_{i=1}^{n} w_i \| \mathbf{R}_l \mathbf{x}_{i,l} - \mathbf{y}_i \|^2 \tag{9a}$$

$$= \underset{\mathbf{R}_l \in SO(3)}{\arg\min} \sum_{i=1}^{n} w_i (\mathbf{x}_{i,l}^\top \mathbf{R}_l^\top \mathbf{R}_l \mathbf{x}_{i,l} - \mathbf{y}_i^\top \mathbf{R}_l \mathbf{x}_{i,l} - \mathbf{x}_{i,l}^\top \mathbf{R}_l^\top \mathbf{y}_i + \mathbf{y}_i^\top \mathbf{y}_i). \tag{9b}$$

As rotation matrices are orthogonal and therefore $\mathbf{R}_l^\top \mathbf{R}_l = \mathbf{I}$, where $\mathbf{I}$ is the identity matrix, and $\mathbf{y}_i^\top \mathbf{R}_l \mathbf{x}_{i,l}$ is a scalar, which implies $\mathbf{y}_i^\top \mathbf{R}_l \mathbf{x}_{i,l} = (\mathbf{y}_i^\top \mathbf{R}_l \mathbf{x}_{i,l})^\top = \mathbf{x}_{i,l}^\top \mathbf{R}_l^\top \mathbf{y}_i$, the optimization problem becomes

$$\mathbf{R}_l = \underset{\mathbf{R}_l \in SO(3)}{\arg\min} \sum_{i=1}^{n} w_i (\mathbf{x}_{i,l}^\top \mathbf{x}_{i,l} - 2\mathbf{y}_i^\top \mathbf{R}_l \mathbf{x}_{i,l} + \mathbf{y}_i^\top \mathbf{y}_i) \tag{10a}$$

$$= \underset{\mathbf{R}_l \in SO(3)}{\arg\min} \sum_{i=1}^{n} -2w_i \mathbf{y}_i^\top \mathbf{R}_l \mathbf{x}_{i,l} \tag{10b}$$

$$= \underset{\mathbf{R}_l \in SO(3)}{\arg\max} \sum_{i=1}^{n} w_i \mathbf{y}_i^\top \mathbf{R}_l \mathbf{x}_{i,l}. \tag{10c}$$

Eq. (10b) holds, as it contains the only term of Eq. (10a) that is depending on $\mathbf{R}_l$ and Eq. (10c) is the equivalent optimization problem. Considering the matrix trace property $\text{Tr}(\mathbf{AB}) = \text{Tr}(\mathbf{BA})$ it can be noted, that

$$\sum_{i=1}^{n} w_i \mathbf{y}_i^\top \mathbf{R}_l \mathbf{x}_{i,l} = \text{Tr}(\mathbf{WY}^\top \mathbf{R}_l \mathbf{X}_l) = \text{Tr}(\mathbf{R}_l \mathbf{X}_l \mathbf{WY}^\top) = \text{Tr}(\mathbf{R}_l \mathbf{S}_l), \quad (11)$$

where $\mathbf{W} = \text{diag}[w_1, \ldots, w_n]$ contains the weights and $\mathbf{S}_l = \mathbf{X}_l \mathbf{WY}^\top$ is the weighted covariance matrix of the centered vectors $\mathbf{x}_{i,l}$ and $\mathbf{y}_i$. By applying the singular value decomposition on $\mathbf{S}_l$, Eq. (11) can be reformulated as

$$\text{Tr}(\mathbf{R}_l \mathbf{S}_l) = \text{Tr}(\mathbf{R}_l \mathbf{U}_l \mathbf{\Sigma}_l \mathbf{V}_l^\top) = \text{Tr}(\mathbf{\Sigma}_l \mathbf{V}_l^\top \mathbf{R}_l \mathbf{U}_l). \quad (12)$$

As $\mathbf{\Sigma}_l$ is a diagonal matrix with non-negative singular values and $\mathbf{V}_l^\top \mathbf{R}_l \mathbf{U}_l$ is orthogonal, Eq. (12) is maximized when $\mathbf{V}_l^\top \mathbf{R}_l \mathbf{U}_l$ is the identity matrix, thus

$$\mathbf{I} = \mathbf{V}_l^\top \mathbf{R}_l \mathbf{U}_l \quad (13)$$

$$\mathbf{R}_l = \mathbf{V}_l \mathbf{U}_l^\top. \quad (14)$$

The optimal orthogonal matrix is calculated with Eq. (14), which covers rotations as well as reflections, where $\det(\mathbf{V}_l \mathbf{U}_l^\top) = +1$ for rotations and $\det(\mathbf{V}_l \mathbf{U}_l^\top) = -1$ for reflections. Noting that the singular values in $\mathbf{\Sigma}$ are arranged in decreasing order and allowing for rotations only, the optimal rotation matrix can finally be calculated as

$$\mathbf{R}_l = \mathbf{V}_l \begin{bmatrix} 1 & 0 & 0 \\ 0 & 1 & 0 \\ 0 & 0 & \det(\mathbf{V}_l \mathbf{U}_l^\top) \end{bmatrix} \mathbf{U}_l^\top. \quad (15)$$

4.2 Extraction of the raw trajectories

With the sequence of poses $\{(\mathbf{R}_1, \mathbf{t}_1), \ldots, (\mathbf{R}_N, \mathbf{t}_N)\}$ a raw trajectory of the horseback motion can be extracted from the movement data, following above method. None of the data sets contained more than one complete gait cycle. Therefore, the pose sequence was cropped to the samples of one single movement cycle per gait. Additionally, as the horses were not necessarily moving parallel to the axes of the reference coordinate system, a trend correction of the translational and rotational components was applied, assuring that start and end of the trajectory are the same. This results in the sampled raw trajectory $\boldsymbol{\tau}$ which is parametrized as

$$\boldsymbol{\tau} = [\mathbf{x}, \mathbf{y}, \mathbf{z}, \boldsymbol{\alpha}, \boldsymbol{\beta}, \boldsymbol{\gamma}]. \quad (16)$$

The samples of the positional components of the rigid body motion with respect to the body fixed reference coordinate frame, as depicted in Fig. 5, are described by $\mathbf{x} = [x_1, \ldots, x_N]^\top$, $\mathbf{y} = [y_1, \ldots, y_N]^\top$ and $\mathbf{z} = [z_1, \ldots, z_N]^\top$. The orientation of the horseback as rotations around the x, y and z axis is described by the Cardan angles $\boldsymbol{\alpha} = [\alpha_1, \ldots, \alpha_N]^\top$, $\boldsymbol{\beta} = [\beta_1, \ldots, \beta_N]^\top$ and $\boldsymbol{\gamma} = [\gamma_1, \ldots, \gamma_N]^\top$ following the rotation sequence X-Y'-Z'' (prime symbols denote the new axis resulting from the previous rotation). Figure 6 shows the extracted raw trajectory of one data set.
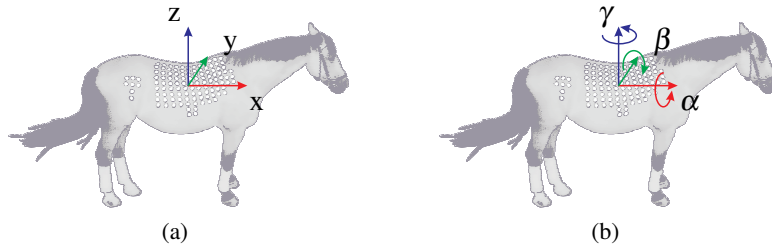

(a)   (b)

Fig. 5: (a) Origin of the body fixed coordinate system, as defined by the reference pose and (b) rotations with respect to this coordinate frame.
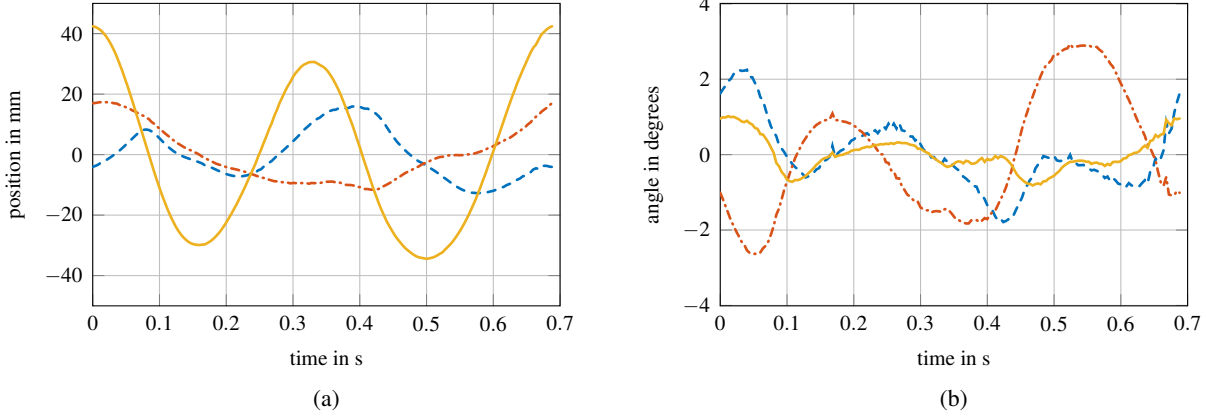
Fig. 6: Extracted raw trajectory for one single movement cycle of the trotting motion (*Lambada*), (a) position in x (dashed blue line), y (dot-dashed red line) and z (solid yellow line) direction and (b) orientation described as Cardan angles α (dashed blue line), β (dot-dashed red line) and γ (solid yellow line).

4.3 Fourier approximation

Due to the cyclic nature of the investigated movements it is reasonable to describe the trajectories as Fourier series

$$f(t) = a_0 + \sum_{k=1}^{m} a_k \cos(k\omega t) + b_k \sin(k\omega t), \quad \omega = \frac{2\pi}{T}. \tag{17}$$

This provides a mathematical description of the trajectory components as input for the robotic system, where T is the period duration of the movement and $\mathbf{a} = [a_0, \dots, a_m]^\top$ and $\mathbf{b} = [b_1, \dots, b_m]^\top$ are the $2m+1$ Fourier coefficients. In order to approximate the raw trajectory, as defined in Eq. (16), the Fourier coefficients for each of its components have to be determined. Therefore, for any trajectory component denoted as $\mathbf{f} \in \{\mathbf{x}, \mathbf{y}, \mathbf{z}, \alpha, \beta, \gamma\}$ Eq. (17) may be reformulated as

$$\mathbf{f} = [\mathbf{\Theta}_1, \dots, \mathbf{\Theta}_N]^\top \begin{bmatrix} \mathbf{a} \\ \mathbf{b} \end{bmatrix} = \mathbf{\Theta}\mathbf{c} \tag{18}$$

with

$$\mathbf{\Theta}_l = [1, \cos(\omega t_l), \dots, \cos(m\omega t_l), \sin(\omega t_l), \dots, \sin(m\omega t_l)]^\top \tag{19}$$

where $l = 1, \dots, N$ again denotes the samples of the data set and t_l are the respecting time instants. This leads to a linear system with the Fourier coefficients $\mathbf{c} = [\mathbf{a}^\top, \mathbf{b}^\top]^\top$ that have to be found. Due to the over-determinacy of Eq. (18), a least squares optimization is used to solve for $\mathbf{c}$. To this end, an error $\mathbf{e}$ and a cost function L, that has to be minimized, are introduced as

$$\mathbf{e} = \mathbf{f} - \mathbf{\Theta}\mathbf{c} \tag{20}$$

$$L = \frac{1}{2}\mathbf{e}^\top\mathbf{e} = \frac{1}{2}\left(\mathbf{f}^\top\mathbf{f} - 2\mathbf{c}^\top\mathbf{\Theta}^\top\mathbf{f} + \mathbf{c}^\top\mathbf{\Theta}^\top\mathbf{\Theta}\mathbf{c}\right). \tag{21}$$

The optimal Fourier coefficients are found by an unconstrained minimization of the cost function through calculating its derivative with respect to $\mathbf{c}^\top$ and searching for the roots, leading to

$$\frac{\partial L}{\partial \mathbf{c}^\top} = -\mathbf{\Theta}^\top\mathbf{f} + \mathbf{\Theta}^\top\mathbf{\Theta}\mathbf{c} = 0 \tag{22}$$

$$\mathbf{c} = (\mathbf{\Theta}^\top\mathbf{\Theta})^{-1}\mathbf{\Theta}^\top\mathbf{f}. \tag{23}$$

By solving Eq. (23) for every positional and rotational component of the raw trajectory τ and therefore obtaining the respective Fourier coefficients, the approximated trajectory of every movement data set can be calculated according to Eq. (17). The result of this approximation approach is shown in Fig. 7.
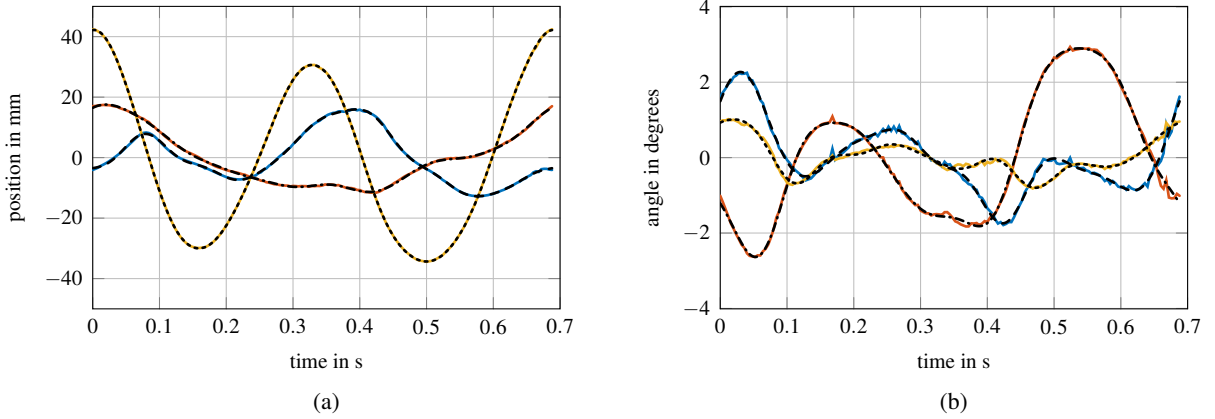
Fig. 7: Comparison of the raw trajectory (solid and colored lines) and the Fourier approximation (broken and black lines) of one movement cycle of the trotting motion (*Lambada*). (a) position in *x* (blue/dashed), *y* (red/dot-dashed) and *z* (yellow/dotted) direction, and (b) orientation described as Cardan angles α (blue/dashed) β (red/dot-dashed) and γ (yellow/dotted).

Extending Eq. (17) by a dilatation parameter ξ, $0 < \xi \leq 1$, easily allows for an adaption of the original trajectory concerning the movement speed according to the therapy requirements or to the capabilities of the robotic system. The dilated version of the approximated trajectory and its first two derivatives can be calculated as

$$f(t) = a_0 + \sum_{k=1}^{m} a_k \cos(k\omega\xi t) + b_k \sin(k\omega\xi t) \tag{24}$$

$$\dot{f}(t) = k\omega\xi \sum_{k=1}^{m} -a_k \sin(k\omega\xi t) + b_k \cos(k\omega\xi t) \tag{25}$$

$$\ddot{f}(t) = k^2\omega^2\xi^2 \sum_{k=1}^{m} -a_k \cos(k\omega\xi t) - b_k \sin(k\omega\xi t). \tag{26}$$

As can be noted in Eq. (25) and Eq. (26), the velocity decreases linearly while the acceleration decreases quadratically with ξ, which might be important considering that the robotic system has to be capable of producing the required actuator forces, e.g. due to the body mass of the patient.

5 Results

Considering the three different horse gaits shown in Fig. 8, the angular displacement of the walking motion seems to be higher than that of the trotting motion. During trotting the vertical movement significantly exceeds the movement in the other two directions, whereas this is not so distinct during walking or galloping. As expected, the highest overall variation of position and orientation occurs when the horse is galloping. Note that singularities due to the utilization of Cardan angles do not occur, as the according angular values are not reached (e.g. $\beta = \pm 90°$). Comparing the trajectories of the two horses, as shown in Fig. 9 and Fig. 10, most of the position and orientation components show reasonable consistency. It has to be mentioned, that the 3D motion capture data covered only one complete motion cycle per gait per horse. Bearing that in mind, a more general characterization of the horseback motion during the different gaits could be achieved by obtaining the mean trajectory of several measurements. Nevertheless, similar results are published in [21, 14] or, when describing the orientation as *yaw-pitch-roll* angles (following the rotation sequence Z-Y'-X"), in [22, 13].

Figure 11 shows a comparison of the position, velocity and acceleration in *z*-direction of the original walking trajectory (*Doolittle*) with an adapted version at 50 % speed ($\xi = 0.5$), therefore in this example the acceleration is scaled to 25 % with respect to the original trajectory.
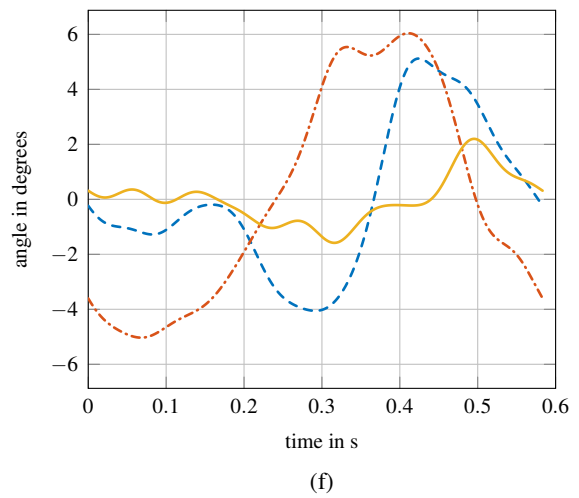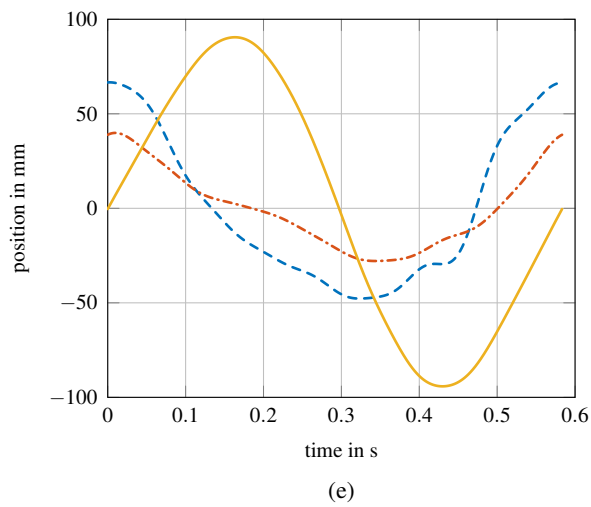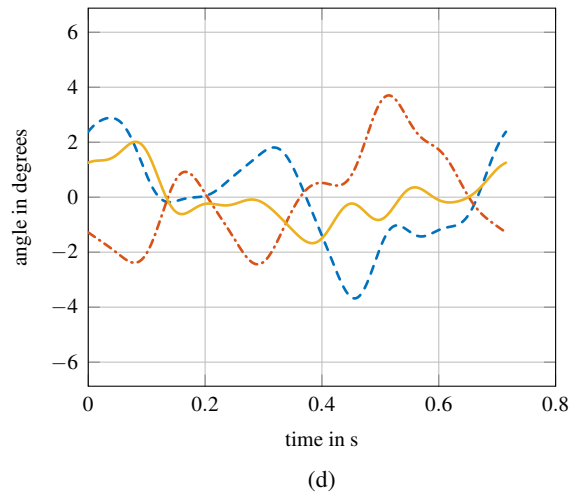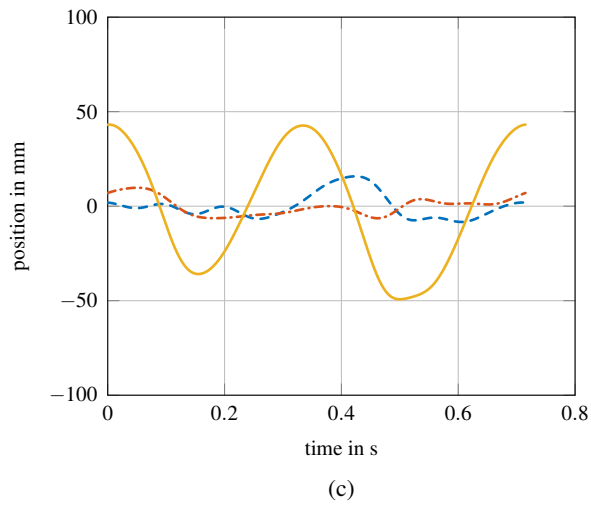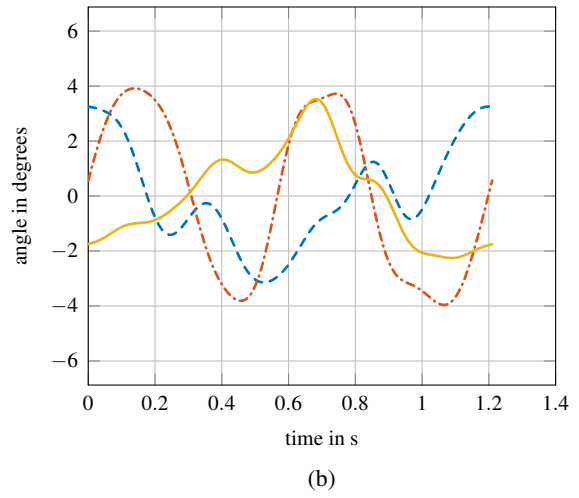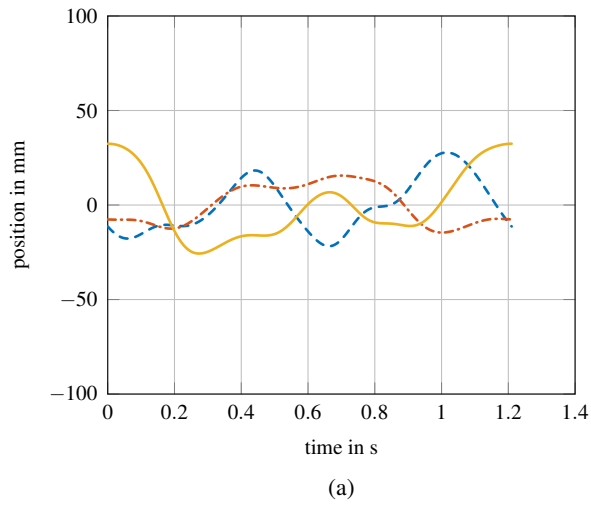
8

Fig. 8: Position (a,c,e) and orientation (b,d,f) of the walking (a,b), trotting (c,d) and galloping (e,f) motion of *Doolittle*, with the *x* position and α angle as dashed blue lines, the *y* position and β angle as dot-dashed red lines and the *z* position and γ angle as yellow solid lines.
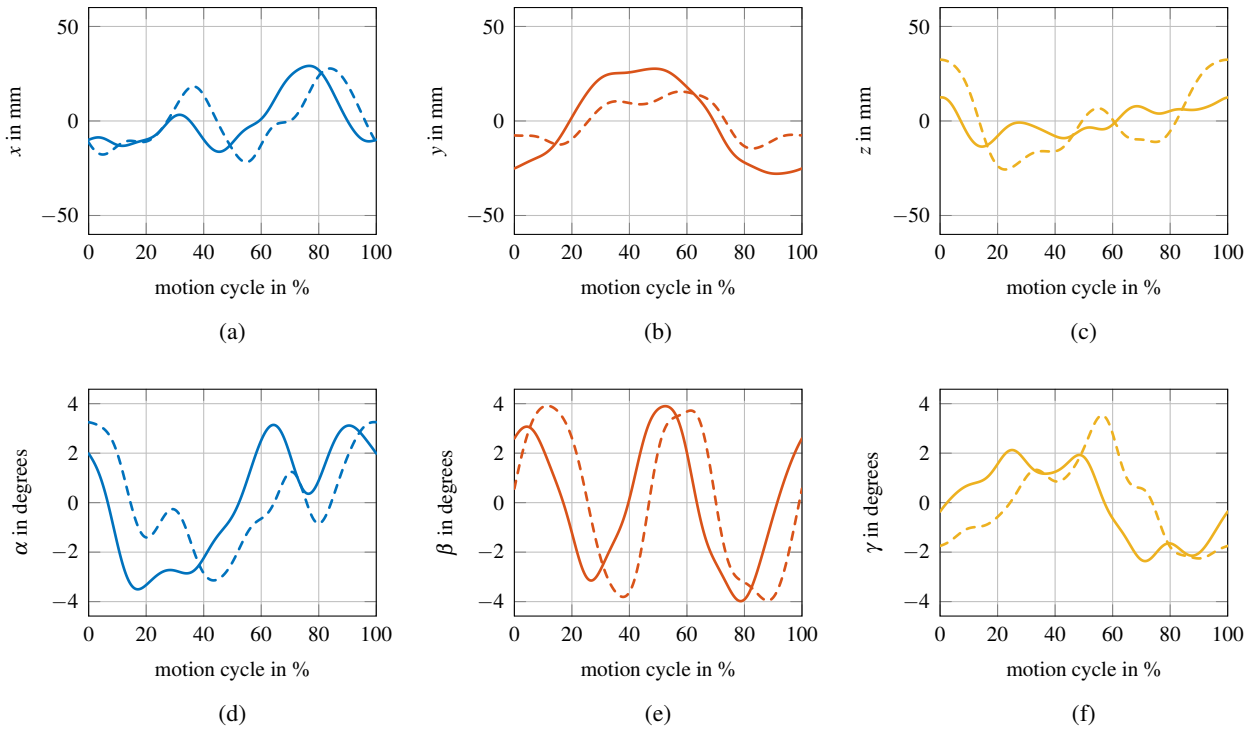
Fig. 9: Comparison of the approximated trajectories of the two horses *Lambada* (solid lines) and *Doolittle* (dashed lines) walking. (a) x position, (b) y position, (c) z position, (d) α angle, (e) β angle and (f) γ angle over one single motion cycle.

Fig. 10: Comparison of the approximated trajectories of the two horses *Lambada* (solid lines) and *Doolittle* (dashed lines) trotting. (a) x position, (b) y position, (c) z position, (d) α angle, (e) β angle and (f) γ angle over one single motion cycle.
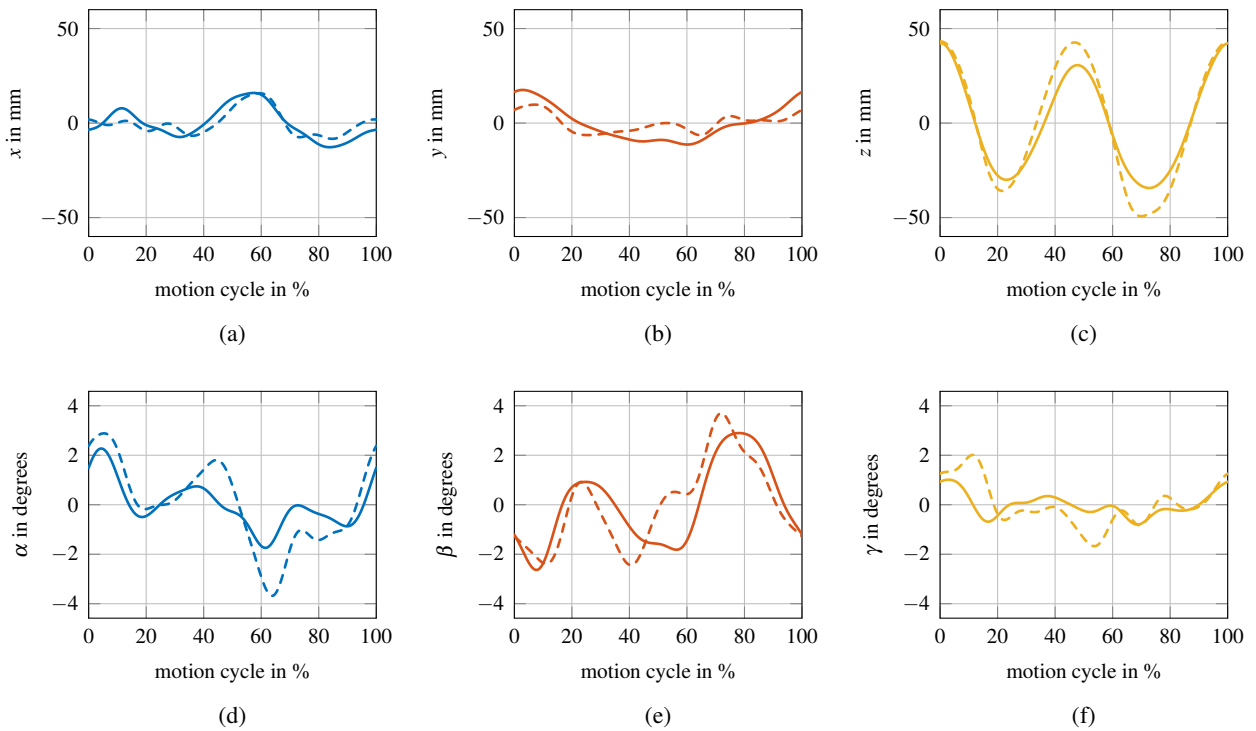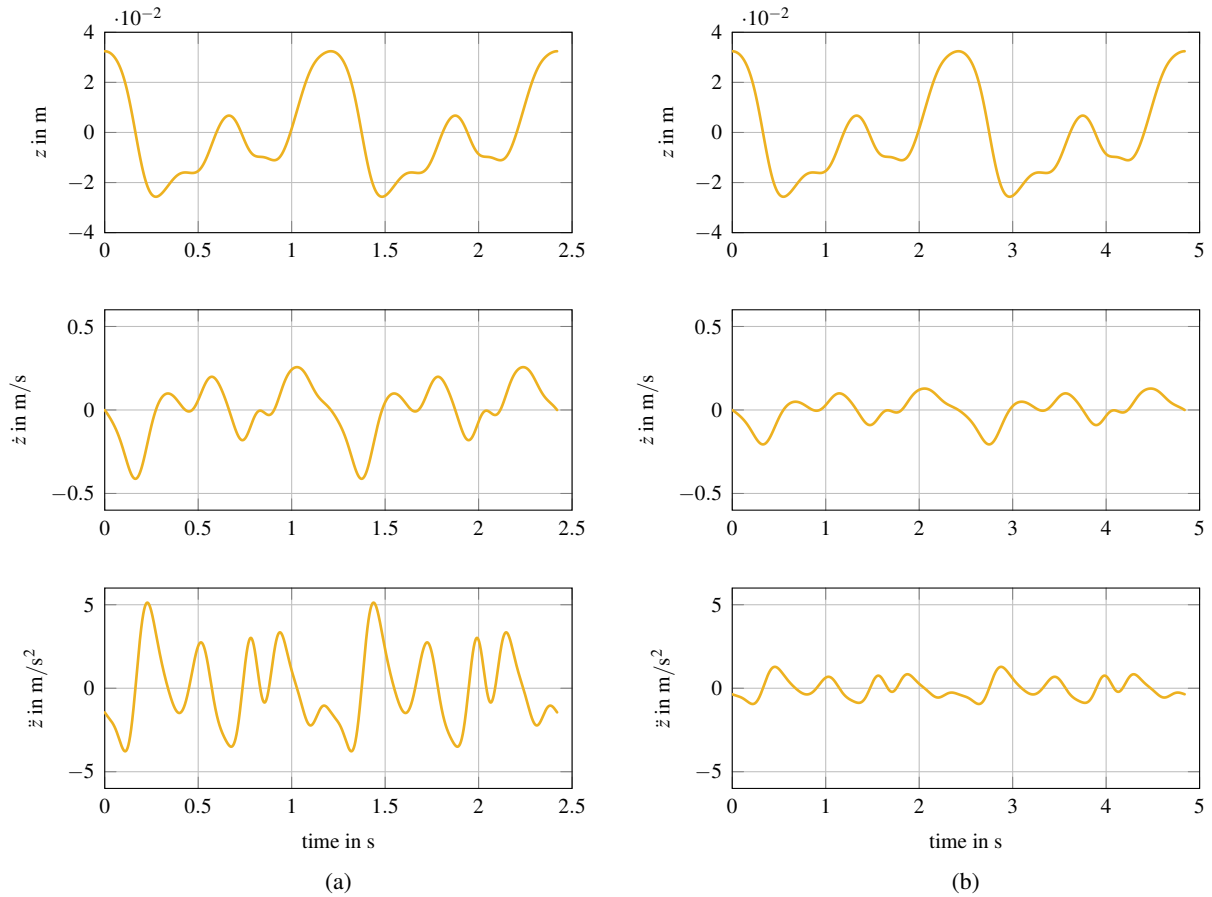
10

Fig. 11: Position, velocity and acceleration (from top to bottom) in *z*-direction of (a) the original walking trajectory (*Doolittle*) and (b) of the same trajectory at 50 % speed.

6 Conclusions

In this paper, 3D motion capture data of two horses moving in three different gaits are processed in order to extract smooth, cyclic trajectories of the horseback. As the horseback is regarded as rigid body representing the saddle of the rehabilitation system, a marker selection approach is introduced to identify the data most significantly describing the respective horse movement. This approach is based on the difference of the marker-to-marker distances between the measurement samples and a defined reference. The rigid motion of the selected markers with respect to the reference throughout the recorded movement data is then calculated in a least squares sense. The resulting raw trajectory consists of position and orientation components, each of which are then approximated by individual Fourier series. Additionally a dilatation parameter is introduced that enables an easy control of the velocity of the trajectory. This allows for the adaption of the generated movement to therapy requirements or to the capabilities of the robotic system.

A comparison of the trajectory components of the same gait for the two horses showed reasonable consistency. It has to be mentioned, that motion capture data of only one complete motion cycle per horse per gait were available. It would be preferable to obtain a mean trajectory for several measurements of the same gait, in order to get a more general characterization of the according horseback motion. Although literature about kinematic analysis concerning horsebacks or saddles is rare, existing publications show similarities to our results.

The presented approach provides an easy and robust method to synthesize horseback motion and to generate smooth, cyclic and realistic trajectories for robotic hippotherapy systems. Based on the trajectories generated with this approach, future research will comprise the design and simulation of a robotic hippotherapy system.

References

[1] H. Uchiyama, N. Ohtani, and M. Ohta, "Three-dimensional analysis of horse and human gaits in therapeutic riding," *Applied animal behaviour science*, vol. 135, no. 4, pp. 271–276, 2011.

[2] B. A. Garner and B. R. Rigby, "Human pelvis motions when walking and when riding a therapeutic horse," *Human movement science*, vol. 39, pp. 121–137, 2015.

[3] J. A. Sterba, B. T. Rogers, A. P. France, and D. A. Vokes, "Horseback riding in children with cerebral palsy: effect on gross motor function," *Developmental Medicine and Child Neurology*, vol. 44, no. 5, pp. 301–308, 2002.

[4] M. Zadnikar and A. Kastrin, "Effects of hippotherapy and therapeutic horseback riding on postural control or balance in children with cerebral palsy: a meta-analysis," *Developmental medicine & child neurology*, vol. 53, no. 8, pp. 684–691, 2011.

[5] T. B. De Araújo, R. J. de Oliveira, W. R. Martins, M. de Moura Pereira, F. Copetti, and M. P. Safons, "Effects of hippotherapy on mobility, strength and balance in elderly," *Archives of gerontology and geriatrics*, vol. 56, no. 3, pp. 478–481, 2013.

[6] W. Benda, N. H. McGibbon, and K. L. Grant, "Improvements in muscle symmetry in children with cerebral palsy after equine-assisted therapy (hippotherapy)," *The Journal of Alternative & Complementary Medicine*, vol. 9, no. 6, pp. 817–825, 2003.

[7] T. L. Shurtleff, J. W. Standeven, and J. R. Engsberg, "Changes in dynamic trunk/head stability and functional reach after hippotherapy," *Archives of physical medicine and rehabilitation*, vol. 90, no. 7, pp. 1185–1195, 2009.

[8] F. Beinotti, N. Correia, G. Christofoletti, and G. Borges, "Use of hippotherapy in gait training for hemiparetic poststroke," *Arquivos de neuro-psiquiatria*, vol. 68, no. 6, pp. 908–913, 2010.

[9] "intelligent motion gmbh." `http://www.intelligentmotion.at`. [Online], accessed: 24.04.2018.

[10] M. A. Elshafey, "Hippotherapy simulator as alternative method for hippotherapy treatment in hemiplegic children," *International Journal of Physiotherapy and Research*, vol. 2, no. 2, pp. 435–441, 2014.

[11] C.-W. Lee, S. G. Kim, and S. S. Na, "The effects of hippotherapy and a horse riding simulator on the balance of children with cerebral palsy," *Journal of physical therapy science*, vol. 26, no. 3, pp. 423–425, 2014.

[12] K.-Y. Kang, "Effects of mechanical horseback riding on the balance ability of the elderly," *Journal of physical therapy science*, vol. 27, no. 8, pp. 2499–2500, 2015.

[13] A. Byström, M. Rhodin, K. Von Peinen, M. Weishaupt, and L. Roepstorff, "Kinematics of saddle and rider in high-level dressage horses performing collected walk on a treadmill," *Equine veterinary journal*, vol. 42, no. 4, pp. 340–345, 2010.

[14] R. Eskola and H. Handroos, "Novel horseback riding simulator based on 6-dof motion measurement, a motion base, and interactive control of gaits," *Advanced Robotics*, vol. 27, no. 16, pp. 1249–1257, 2013.

[15] T.-C. Huang, Y.-J. Huang, and W.-C. Lin, "Real-time horse gait synthesis," *Computer Animation and Virtual Worlds*, vol. 24, no. 2, pp. 87–95, 2013.

[16] P. H. Schönemann, "A generalized solution of the orthogonal procrustes problem," *Psychometrika*, vol. 31, no. 1, pp. 1–10, 1966.

[17] K. S. Arun, T. S. Huang, and S. D. Blostein, "Least-squares fitting of two 3-d point sets," *IEEE Transactions on pattern analysis and machine intelligence*, no. 5, pp. 698–700, 1987.

[18] B. K. Horn, "Closed-form solution of absolute orientation using unit quaternions," *Journal of the Optical Society of America A*, vol. 4, no. 4, pp. 629–642, 1987.

[19] B. K. Horn, H. M. Hilden, and S. Negahdaripour, "Closed-form solution of absolute orientation using orthonormal matrices," *Journal of the Optical Society of America A*, vol. 5, no. 7, pp. 1127–1135, 1988.

[20] O. Sorkine-Hornung and M. Rabinovich, "Least-squares rigid motion using svd," Technical Report, Department of Computer Science, ETH Zurich, 2017.

[21] S. Warner, T. Koch, and T. Pfau, "Inertial sensors for assessment of back movement in horses during locomotion over ground," *Equine Veterinary Journal*, vol. 42, no. s38, pp. 417–424, 2010.

[22] A. Byström, M. Rhodin, K. v. Peinen, M. Weishaupt, and L. Roepstorff, "Basic kinematics of the saddle and rider in high-level dressage horses trotting on a treadmill," *Equine veterinary journal*, vol. 41, no. 3, pp. 280–284, 2009.